Reduction of iron oxides by carbon in a circulating fluidized bed reactor

Iyengar, Srinivasan

Published in:
Powder Technology

DOI:
10.1016/S0032-5910(01)00484-3

2002

ELSEVIER

Powder Technology 124 (2002) 28–39

POWDER TECHNOLOGY

www.elsevier.com/locate/powtec

Reduction of iron oxides by carbon in a circulating fluidized bed reactor

N.S. Srinivasan*

Division of Materials Engineering, Lund University, P.O. Box 118, 221 00, Lund, Sweden

Received 1 May 2001; received in revised form 3 September 2001; accepted 17 September 2001

Abstract

A theoretical analysis of the reduction of iron oxides by carbon in a circulating fluidized bed reactor is considered in this study. Iron oxide and coal particles are fast fluidized in the main column by a hot stream of gases ($N_2-CO-CO_2-H_2-H_2O$). The analysis considers kinetic and hydrodynamic factors in the reactor and assumes the reduction reaction by carbon to proceed through gaseous intermediates.

Using reported base data, the model has been used to generate the temperature and composition profiles in the charge as well as the gas phase, both in the main as well as return columns. Under these conditions, the change in oxygen content of an isolated iron oxide particle during its passage through the CFB has been computed. The results indicate that a freshly introduced oxide particle needs to circulate in the system five to six times before the reduction level approaches about 60%.

Keywords: Iron oxide; Reduction; Kinetics; Modeling; Circulating fluidized bed

1. Introduction

Iron ores have been reduced in the solid state in a variety of reactors such as retorts, shaft furnaces, rotary kilns and fluidized beds to produce Direct Reduced Iron (DRI) [1]. By and large, these processes are based on the use of lump ores or pellets, with exceptions like the Höganäs process and fluidized bed processes [1,2]. The reducing agent used is either a reducing gas or coal. DRI is primarily used as a substitute for scrap in steelmaking.

Focus on the processing of low cost iron ore fines has increased significantly during the last three decades especially with the pilot scale development of the smelting reduction processes for the production of liquid iron [3–6]. In these processes, iron ore is partially reduced at relatively low temperatures in the first stage and the reduction is completed followed by melting in the final stage at a much higher temperature. The plasmasmelt process [3] envisages the gaseous prereduction of iron ore fines in a series of bubbling fluidized beds at about 800 °C and final reduction and melting in a low shaft reactor equipped with plasma guns. Even in the Kawasaki process [4] for hot metal production, prereduction is carried out in bubbling fluidized beds and final reduction and melting in a reactor where coal is gasified to CO to meet the needs of energy and reduction. In the ELRED process [5,6], prereduction of iron ore fines is carried out in a circulating fluidized bed reactor (CFB) with coal as the reducing agent at 950 to 1000 °C and the partially reduced material enters a DC-arc furnace for final reduction and melting.

The two-stage reduction concept has also been used to develop processes to produce DRI using iron ore fines. The Circored and Circofer processes [7–9] use a CFB for prereduction up to 70% (short residence time) and a bubbling fluidized bed reactor for final reduction (long residence time). The Circored process uses hydrogen as the only reducing agent while Circofer is a coal-based process.

Although the above-mentioned processes have not been commercialized so far, a breakthrough for such processes based on iron ore fines is a distinct possibility in the near future, as the economic and environmental advantages are gaining ground quickly compared to the conventional methods of ironmaking [10,11]. Further, the concept of two-stage processing in different reactors offers interesting possibilities for modeling and optimization. In this connection, the gaseous reduction of iron ores in bubbling fluidized beds was analyzed in an earlier study [12]. In this work, a theoretical analysis of the reduction of iron oxides by carbon in a CFB is considered.

2. Circulating fluidized bed reactors

During the last 20 years, interest in fluidization regimes other than the conventional bubbling bed has grown steadily

* Tel.: +46-46-222-79-84; fax: +46-46-222-46-20.
E-mail address: srini@material.lth.se (N.S. Srinivasan).

0032-5910/02/$ - see front matter
PII: S0032-5910(01)00484-3

[13,14]. The advantages of high velocity fluidization over bubbling fluidization are now well recognised. Circulating fluidized bed reactors employing high superficial gas velocities are now used for industrial applications such as calcination of alumina, prereduction of iron ores, coal gasification etc. [15,16]. However, a complete understanding of high velocity fluidization is still lacking at present unlike that for bubbling fluidization.

The circulating fluidized bed reactor with its attractive features has been found suitable for a wide range of gas–solid reactions. In the fast fluidizing condition, the gas–solid contacting efficiency is higher relative to a bubbling fluidized bed reactor. In addition, the CFB reactor offers good heat transfer characteristics and thermal control. The gas is approximately in plug flow and the solids are in a well mixed condition. The recycling of solids leads to better mixing among the solids.

Grace et al. [17] have presented design and operating data for a laboratory CFB reactor used for the combustion of solid and liquid fuels. Their studies were aimed at relating reaction characteristics to reactor hydrodynamics and transfer processes. They have reported heat transfer data, temperature and pressure profiles for typical coal combustion. They observed that during combustion, the temperature rises slowly in the main reactor. A slight decrease in temperature is associated with the return leg of the reactor, as expected. No radical change in the bed hydrodynamics was observed with increase in operating temperature. The authors point out that radial mixing in the gas phase may be slow if the gas inlet ports are only few.

Dry et al. [18] studied the gas–solids contact efficiency in high velocity fluidized beds using a laboratory reactor (~ 9 cm diameter, 2 to 8 m/s gas velocity and a solids recirculation rate of up to 200 kg/m^2 s). They observed that the gas–solids contact is almost complete at a gas velocity of 2 m/s for solids recirculation rates exceeding 100 kg/m^2 s. They noted that the contact efficiencies could be significantly less than 100% at very high gas velocities.

Basu et al. [19] have examined the burning rates of coarse carbon particles (>1 mm) in a circulating fluidized bed of fine solids (sand particles). Their results from a 10-cm diameter fast bed indicates that the overall burning rates for carbon particles as large as 3 to 5 mm in diameter lie close to the kinetic limit. This suggests a very high rate of mass transfer to coarse particles distributed in a fast bed of fine solids.

Grace [20] has pointed out that the understanding of heat transfer from circulating beds is at an early stage. Based on available data, he has estimated that the surface to suspension heat transfer coefficient is likely to be about 150 to 250 W/m^2 K. The particle convective component is of major importance. Radiation assumes importance at high temperatures and dilute suspensions. Grace has shown that particles injected into a circulating bed adjust to the suspension temperature in a single pass. Intraparticle temperature gradients are likely to be minor under normal operating conditions. Further, Grace has shown that gas introduced at one temperature quickly attains the bulk particle temperature within a relatively short distance. Hence, the bed tends to be nearly isothermal except for shallow regions near the inlet ports and individual reacting particles. Strömberg [21] has clearly demonstrated the uniformity of temperature in a fast bed for a CFB combustor.

In order to determine the heat transfer coefficient when voids are in contact with the wall, Subbarao and Basu [22] suggested a model based on the packet theory of Mickley and Fairbanks [23] and considered transient conduction of heat to the semi-infinite void space between the clusters. The cluster renewal theory leads to the prediction of low values of the heat transfer coefficient relative to experimentally obtained data [24]. It is clear that in between contacts with two successive clusters, the wall is in contact with a dilute phase flowing upwards, with a continuously developing boundary layer on the wall. Basu and Nag [25] have modified the model by including a contact resistance at the wall due to the build up of a gas film whose thickness is proportional to the particle diameter. Model predictions appear to be in good agreement with observed wall heat transfer data.

The hydrodynamic behaviour of fast fluidized beds has been studied by several workers. Li and Kwauk [26] have proposed a mathematical model to describe the axial voidage profiles under fast fluidization conditions. The model assumes the presence of clusters in a dense phase at the bottom of the bed. These clusters are projected upward into a relatively dilute phase and eventually fall back due to buoyancy forces. The model results in an S-shaped curve for the voidage profile in the bed, with the voidage tending to limiting values in the dense and dilute phase regions of the bed.

Rhodes and Geldart [27,28] have proposed a model for the hydrodynamics of circulating fluidized beds. The authors have combined existing entrainment and bed expansion correlations with a pressure balance for the system. Model predictions show qualitative agreement with experimental data for a Group A powder over a wide range of gas velocities and solid recirculation rates.

While several applications have been developed for carrying out gas–solid reactions in CFB reactors, very few attempts have been made to model such reactions. Weiss et al. [29] have proposed a model for describing CFB reactors. It is based on a simulation method for conventional bubbling fluidized beds. The reactor, cyclone and heat exchanger are considered as individual compartments (cells) arranged one above the other. The cell model assumes backmixing of solids and neglects the effect of bubbles, clouds and clusters. The wall temperature is considered to be constant in each cell. The authors have applied the model to data on the thermal decomposition of sodium bicarbonate in a laboratory circulating fluidized bed. A good agreement was observed between predicted conversions and experimental data. The authors also report

successful application of the model to pilot plant data on the combustion of coal in a CFB reactor.

This paper considers the the development of a theoretical approach to the partial reduction of iron ore fines by carbon in a CFB reactor. The conditions in the reactor are assumed to correspond approximately to those in the prereduction stage of the Circofer [7–9] or Elred [5,6] process. During prereduction, iron ore is reduced to about 50% to 60% in the presence of excess carbon, which prevents sticking in the bed. Reducing gases are generated in situ by oxidizing carbon with a controlled supply of air. The gases leaving the CFB reactor are cooled, cleaned and partially reused as the fluidizing gas. Kinetic and hydrodynamic factors in the CFB reactor are considered in the development of the model.

3. Theoretical approach

Fig. 1 shows a schematic diagram of the CFB reactor as envisaged. It essentially consists of a main column in which the iron ore–coal mixture is fluidized at high velocity and a return column in which the entrained solids from the main column are collected via a cyclone. Solids from the return column are recirculated to the bottom of the bed in the main column through a control valve. Fast bed conditions prevail in the main column and the solids in the return column constitute the slow bed. Solids are continuously fed in at the top of the reactor and enter the slow bed through the cyclone. During this descent, the solids get preheated by the rising gases. Partial reduction of the higher oxides of iron also takes place. As a first approximation, the starting material in the ore feed is assumed to be wüstite.

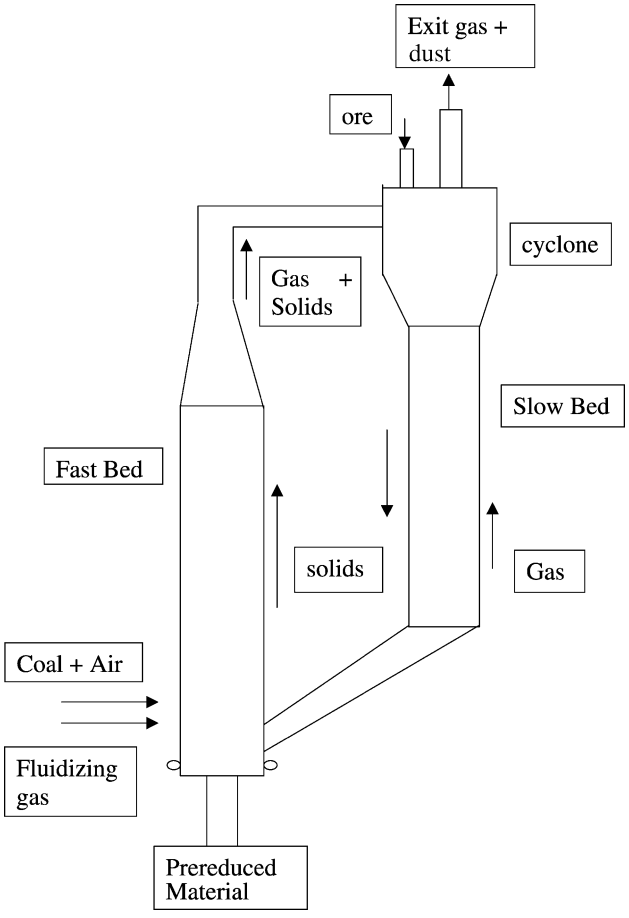

Fig. 1. Schematic diagram of the circulating fluidized bed reactor.

For purposes of analysis, iron oxide and coal particles of specified characteristics (composition, size distribution, porosity and reactivity) are considered to be fast fluidized in the main column by a hot gas stream (N_2–CO–CO–H_2–H_2O). The gas is considered to be in plug flow and the solids are assumed to be well mixed. Further, it is assumed that oxygen from the air injected is consumed instantaneously due to fast oxidation reactions and the gas phase contains negligible free oxygen.

3.1. Reaction scheme

The reactions associated with the reduction of wüstite to iron can be written as:

$$Fe_xO + C = xFe + CO \quad (1)$$

$$Fe_xO + CO(g) = xFe + CO_2(g) \quad (2)$$

$$Fe_xO + H_2(g) = xFe + H_2O(g) \quad (3)$$

$$C + CO_2(g) = 2CO(g) \quad (4)$$

$$C + H_2O(g) = CO(g) + H_2(g) \quad (5)$$

$$C + O_2(g) = CO_2(g) \quad (6)$$

Reaction (1) is significant only at low pressures [30]. Gaseous reduction reactions (2) and (3) predominate at ordinary pressures and reduction proceeds through gaseous intermediates. The regeneration of CO and H_2 takes place through reactions (4) and (5). Of the gasification reactions (4)–(6), reaction (4) is the slowest and could be rate limiting in the temperature interval 1075 to 1275 K.

3.2. Reduction of iron oxide by CO and H_2

Several general models have been proposed in the literature for describing the kinetics of gas–solid reactions [31,32]. In this work, for simplicity, it is assumed that the shrinking core model [33] describes adequately the reduction behaviour of iron oxide particles. The following steps are envisaged in the overall reduction reaction.

(a) Mass transfer across the gaseous boundary layer surrounding the particle
(b) Diffusion of gases through the porous product layer
(c) Chemical reaction between the reactant gas and the unreduced oxide at the reaction interface.

The above scheme considers a single reaction interface which is consistent with the step-wise reduction of iron oxides. This type of reduction behaviour has been observed in practice especially for fine iron oxide particles.

In the general case, the reduction reaction will be under mixed control kinetics if the transport as well as the chemical reaction steps are important. Assuming first order reversible kinetics for the chemical reaction, the rate of oxygen removal from a dense and spherical iron oxide particle can be written as:

$$-\dot{n}_0 = \frac{\left[p_A^b - p_B^b/K_{eq}^A\right]/RT}{\left[1/\alpha^{(A)}4\pi r_0^2\right] + (r_0 - r_i)/\left[\beta^{(A)}4\pi r_i r_0\right] + \left[1/k_r^{(A)}4\pi r_i^2\right]} \quad (7)$$

where the indices (A) and (B) refer to the reducing gas (A) and the product gas (B).

$$\alpha^{(A)} = K_{eq}^A k_m^A k_m^B / \left[K_{eq}^A k_m^B + k_m^A\right] \quad (8)$$

$$\beta^{(A)} = K_{eq}^{(A)} D_A^{eff} D_B^{eff} / \left[K_{eq}^{(A)} D_B^{eff} + D_A^{eff}\right] \quad (9)$$

Using Eq. (1), the rate of advance of the reaction front can be written as:

$$\frac{dr_i}{dt} = -\left[p_A^b - p_B^b/K_{eq}^A\right] k_{OV}^A/RTC_0 \quad (10)$$

where

$$k_{OV}^{(A)} = \left[(r_i^2/\alpha^{(A)} r_0^2) + r_i(r_0 - r_i)/\beta^{(A)} r_0 + 1/k_r^{(A)}\right]^{-1} \quad (11)$$

and C_0 is the initial molar density of oxygen in the particle.

For the case of reduction by a mixture of gases like CO and H_2, Eq. (10) can be suitably modified to include both contributions as follows:

$$\frac{dr_i}{dt} = -(1/RTC_0)\left[\left(p_{CO}^b - p_{CO_2}^b/K_{eq}^{CO}\right)k_{OV}^{(CO)} + \left(p_{H_2}^b - p_{H_2O}^b/K_{eq}^{(H_2)}\right)k_{OV}^{(H_2)}\right] \quad (12)$$

The rate of movement of the reaction front can be related to the rate of change of fractional removable oxygen in the particle at any given time by the equation

$$\frac{dr_i}{dt} = \left(\frac{r_0}{3}\right) f_0^{-\frac{2}{3}} \frac{df_0}{dt} \quad (13)$$

3.3. Gasification of carbon

In a gas stream comprising of O_2, CO, CO_2, H_2 and H_2O, gasification of carbon can take place through several reactions. These include: C–O_2, C–H_2O, C–CO_2, C–H_2 reactions. These reactions have been studied extensively [34] and it is generally accepted that the carbon–oxygen reaction proceeds very fast relative to the other reactions. On the other hand, the carbon–hydrogen reaction resulting in the formation of methane is very slow and can be neglected. Hence, assuming that the carbon–oxygen reaction goes to completion, carbon gasification can be adequately described by taking into account the carbon–steam reaction and the carbon–carbondioxide (Boudouard) reaction.

According to Ergun [35], an oxygen exchange reaction takes place on the surface of carbon immediately on exposure to CO_2 or H_2O. The surface reactions can be written as:

$$C_f + CO_2(g) \underset{k'_{14}}{\overset{k_{14}}{\rightleftarrows}} C(O) + CO(g) \quad (14)$$

$$C_f + H_2O(g) \underset{k'_{15}}{\overset{k_{15}}{\rightleftarrows}} C(O) + H_2(g) \quad (15)$$

where C_f is a free reaction site on the carbon surface and C(O) represents an occupied reaction site where an oxygen atom is adsorbed.

Reactions (14) and (15) are quite fast and proceed to equilibrium [35,36]. The rate limiting step in the gasification reaction is the desorption of CO(g) from an occupied reaction site, which can be written as:

$$C(O) \overset{k_{16}}{\rightarrow} CO(g) + C_f \quad (16)$$

Based on the above mechanism, the carbon gasification rate in the presence of CO and CO_2 only can be expressed as

$$\text{rate} = k_{ct} I_3 X_{CO_2}/(1/P_T + I_2 X_{CO} + I_3 X_{CO_2}) \quad (17)$$

where k_{ct} is a rate constant characterisic of the type of carbon,

$$I_2 = k'_{14}/k_{16} \quad (\text{atm}^{-1})$$

$$I_3 = k_{14}/k_{16} \quad (\text{atm}^{-1})$$

I_2 and I_3 are constants which are independent of the type of carbon.

Similarly, in the presence of a gas mixture containing only H_2 and H_2O, the rate of carbon gasification can be written as:

$$\text{rate} = k'_{ct} I'_3 X_{H_2O}/(1/P_T + I'_2 X_{H_2} + I'_3 X_{H_2O}) \quad (18)$$

where k'_{ct} is the characteristic rate constant,

$I'_2 = k'_{15}/k_{16}$ (atm^{-1})
$I'_3 = k_{15}/k_{16}$ (atm^{-1})

In a $CO-CO_2-H_2-H_2O$ gas stream, the total gasification rate can be approximately expressed as [37]:

$$\text{total gasification rate} = (k_{ct} I_3 X_{CO_2} + k'_{ct} I'_3 X_{H_2O}) / (1/P_T + I_2 X_{CO} + I_3 X_{CO_2} + I'_2 X_{H_2} + I'_3 X_{H_2O}) \quad (19)$$

It has been observed that the carbon–steam reaction is about three times faster relative to the carbon–carbondioxide reaction at about 800 °C [34]. However, the temperature dependence of the two reaction rates have been found to be similar.

3.4. Reactor modelling

It is well known that the main column (fast bed) and the return column (slow bed) of the CFB reactor are associated with widely different hydrodynamic conditions. The fast bed is associated with high gas velocities, low concentration of solids and well mixed solids. Excellent mass transfer characteristics and near isothermal conditions prevail. On the other hand, approximately packed bed conditions exist in the slow bed and there is a temperature gradient across the bed. Reactions proceed to different extents in each reactor column and the overall conversion of solids is determined by the residence time of solid particles in the two legs of the reactor. It is therefore convenient to model the reactor in two stages taking into account the relevant kinetic and hydrodynamic factors in each stage. This approach has been taken in the present work.

3.5. The fast bed

The model envisages fine iron oxide particles and relatively coarser coal char particles to be well mixed under isothermal conditions in the fast bed. Segregation in the bed is neglected. Water gas equilibrium is assumed to prevail in the gas phase which is considered to be in plug flow.

In general, when a mixture of solids is fluidized, the minimum fluidization velocity of one specie will be lower than the other. Several correlations have been proposed in the literature for calculating the U_{mf} of mixtures. One of the successful equations proposed is due to Cheung et al. [38] and is given below for a binary mixture.

$$[U_{mf}]_{mix} = U_{low}\left(\frac{U_{high}}{U_{low}}\right)^n \quad (20)$$

where $n = (x_{high})^2$

Although Eq. (20) was originally proposed for binary mixtures of equal density, Nienow and Chiba [39] have shown that the equation can be extended to multicomponent systems and can also be applied to mixtures with a density difference if there is no strong segregation tendency. In flotsam-rich systems (as in the present case), it has been reported that there is uniform mixing in the bed as the gas velocity is increased well beyond the minimum fluidization velocity for the mixture.

The variation of U_{mf} with the imposed flux of solids (G) can be estimated using the following equation.

$$[U_{mf}]_{mix} = [U_{mf}]_{G=0} + \left(\frac{G}{\rho_s}\right)\frac{\varepsilon_{mf}}{(1-\varepsilon_{mf})} \quad (21)$$

where $n = (x_{high})^2$.

In order to calculate the voidage profile in the fast bed, the method of Rhodes and Geldart [27], based on the entrainment of solids, has been adopted. They assumed that the fast bed contains a region of dense-phase transport followed by a region of dilute phase transport. The position of the dilute-phase/dense-phase interface is determined in such a way that the entrainment flux at the reactor outlet is equal to the imposed solids circulation flux. The relevant equations are given below.

The variation of the entrainment flux (E) over a fluidized bed is given by the equation [40],

$$E = E_\infty + (E_0 - E_\infty)\exp(-ah) \quad (22)$$

where h refers to the height above the bed and a is a constant.

At the reactor outlet ($h = h^*$),

$$G = \text{imposed flux} = E_\infty + (E_0 - E_\infty)\exp(-ah^*) \quad (23)$$

Wen and Chen [40] have suggested the following correlations for E_0 and E_∞, the entrainment fluxes at the bed surface and above the transport disengaging height.

$$\left(\frac{E_0}{Ad_b}\right) = 3.07\cdot 10^{-9}\left(\frac{\rho_g^{3.5} g^{0.5}}{\mu_g^{2.5}}\right)(U_0 - U_{mf})^{2.5} \quad (24)$$

$$E_\infty = \rho_s(1-\varepsilon_i)(U_0 - U_t) \quad (25)$$

where d_b is the bubble diameter at the surface of the bubbling bed (dense phase) and is given by the relationship [41]:

$$d_{b,h} = 0.54(U_0 - U_{mf})^{0.4}\left[h_{bed} + 4A_0^{0.5}\right]^{0.8}/g^{0.2} \quad (26)$$

where $h_{bed} = h_{fb} - h^*$.

$$\varepsilon_i = \left[1 + \left\{\lambda(U - U_t)^2/(2gd_b)\right\}\right]^{-1/4.7}$$

and λ is calculated from:

$$\left(\frac{\lambda\rho_s}{d_p^2}\right)\left(\frac{\mu_g}{\rho_g}\right)^{2.5} = 5.17Re_p^{-1.5}D^2 \text{ for } Re_p \le Re_{p,c}$$

$$= 12.3Re_p^{-2.5}D \text{ for } Re_p \ge Re_{p,c}$$

$$Re_p = \rho_g(U_0 - U_t)d_p/\mu_g$$

and

$$Re_{p,c} = 2.38/D$$

Assuming that the slip velocity is equal to the single particle terminal velocity, Rhodes and Geldart [27] have derived the following equation:

$$U_t\varepsilon_h^2 + \varepsilon_h(U_0 + U_t + E_h/\rho_s) + U_0 = 0 \quad (27)$$

With a knowledge of U_0, ρ_s and U_t, the vertical voidage profile can be calculated using the above equation for a given entrainment flux. The mass of solids in the dilute phase of the bed can be calculated from:

$$M_{dil} = \int_{h=0}^{h=h^*} \rho_s(1-\varepsilon_h)A_{fb}\,dh \quad (28)$$

Treating the dense phase region in the fast bed as a bubbling fluidized bed, we can write:

$$\varepsilon_{den} = \delta\varepsilon_b + (1-\delta)\varepsilon_e \quad (29)$$

where: δ = bubble fraction in the dense phase = $(U_0 - G/\rho_s - U_{mf})/U_b$; ε_e = voidage in the emulsion phase $\approx \varepsilon_{mf}$; ε_b = voidage in the bubble phase ≈ 1.

The bubble velocity is given by,

$$U_b = U_0 - \left(\frac{G}{\rho_s}\right) - U_{mf} + 0.711(gd_b)^{0.5} \quad (30)$$

The mass of the dense phase can now be written as:

$$M_{den} = \rho_s(1-\varepsilon_{den})(h_{fb} - h^*) \quad (31)$$

Neglecting wall friction effects, the total pressure loss in the fast bed can be expressed as:

$$\Delta P_{fb} = \frac{(M_{dil} + M_{den})g}{A_{fb}} + \frac{G^2}{\rho_s(1-\varepsilon_{dil})} \quad (32)$$

A pressure balance for the reactor gives:

$$\Delta P_{sb} = \Delta P_{fb} + \Delta P_{cyc} + \Delta P_{valve} \quad (33)$$

With a knowledge of the pressure drop in the cyclone and the circulation valve, the required pressure drop in the slow bed can be obtained from Eqs. (32) and (33).

The general mass balance equation for the gaseous species can be written as

$$\frac{d}{dz}(\dot{N}_i) + \dot{r}_{g,i} = 0 \quad (34)$$

where $\dot{r}_{g,i}$ is the net rate of generation of ith gaseous species per unit bed volume.

For the various species, the net rate of generation is given by

$$\dot{r}_{g,CO} = \dot{r}_{[4]} + 2\dot{r}_{[5]} - \dot{r}_{[2]} \quad (35)$$

$$\dot{r}_{g,CO_2} = \dot{r}_{[2]} - \dot{r}_{[4]} \quad (36)$$

$$\dot{r}_{g,H_2} = \dot{r}_{[5]} - \dot{r}_{[3]} \quad (37)$$

$$\dot{r}_{g,H_2O} = \dot{r}_{[3]} - \dot{r}_{[5]} \quad (38)$$

$$\dot{r}_{g,N_2} = 0 \quad (39)$$

where $\dot{r}_{[i]}$ is the rate of ith reaction per unit bed volume.

The variation of pressure as a function of bed height can be expressed as

$$\frac{d}{dz}(P_T) = \rho_s\left[1 - \varepsilon_{fb}(z)\right]g \quad (40)$$

It is well known that the gas phase quickly attains the temperature of the solids at the bottom of the bed [20]. Ignoring heat losses, the variation of solids temperature in the axial direction is given by

$$\frac{d}{dz}(T_s) = -\sum \dot{r}_{[i]}\Delta H_{[i]}/(U_s(z)C_{p,s}) \quad (41)$$

The above system of equations can be solved numerically to obtain axial profiles of degree of reduction, gas composition, etc. in the fast bed.

3.6. The slow bed

The circulating bed of material leaving the fast bed passes through a cyclone and is collected in the return leg of the reactor which is called the slow bed. Packed bed conditions exist in the slow bed and there is a counter-current flow of gases generated inside the bed. The upward gas stream leaving the reactor heats up the incoming iron ore feed and also partially reduces it. As a first approximation, the model assumes that the iron ore particles in the feed that enter the slow bed are wüstite particles.

The mass and height of the slow bed are given by

$$M_{sb} = \Delta P_{sb}A_{sb}/g \quad (42)$$

$$H_{sb} = M_{sb}/\left[\rho_s A_{sb}(1-\varepsilon_{sb})\right] \quad (43)$$

The downward velocity of solids can be expressed as:

$$U_s = \frac{(GA_{fb} + F_{ore})}{\rho_s A_{sb}(1 - \varepsilon_{sb})} \quad (44)$$

Assuming a linear variation of pressure in the bed,

$$\frac{d}{dz}(P_T) = \rho_s(1 - \varepsilon_{sb})g \quad (45)$$

Temperature variations in the bed can be described for the solid species by:

$$\frac{d}{dz}(T_s) = \left[a_s h_c(T_s - T_g) - \sum \dot{r}_{[i]}\Delta H_{[i]}\right]/(V_s C_{p,s}) \quad (46)$$

and for the gaseous species by:

$$\frac{d}{dz}(T_g) = a_s h_c(T_g - T_s)/\left(\sum \dot{N}_i C_{p,g}\right) \quad (47)$$

4. Solution of equations

The system of equations presented in the preceding section forms the basis of the analysis of reduction in the CFB reactor. The equations representing various phenomena can be solved using the following scheme.

4.1. Calculation scheme

(a) Fast bed calculations.
the temperature and composition of the solids and gases at the bottom of the bed are assumed to be known.

(i) For a given entrainment flux, the minimum fluidization velocity of the mixture of solids in the fast bed is calculated (Eqs. (20) and (21)). Then, using Eqs. (22)–(27), the vertical voidage profile in the bed is determined for a specified gas velocity.
(ii) Mass of the dilute and dense phase regions of the bed are calculated using Eqs. (28) and (31). The total pressure loss in the fast bed is estimated using Eq. (32).
Using estimates for the pressure drop in the cyclone and the circulation valve, the required pressure drop in the slow bed is calculated (Eq. (33)). The dimensions of the slow bed can now be calculated.
(iii) Using Eqs. (12), (13), (19), (34)–(41), the compositional variations in the solid and gaseous phases, temperature and pressure are determined as a function of bed height.

(b) Slow bed calculations.
the temperature and composition of the charge at the top of the slow bed are taken to be the same as that for the material leaving the fast bed.
A finite gas flow rate is assumed at the bottom of the slow bed. The composition of the gas, its temperature and pressure are assumed to be the same as that for the fluidizing gas in the fast bed.
The dimensions of the slow bed are determined using Eqs. (42) and (43) and the calculated value of the pressure drop from the previous section.
Variations in composition and temperature of the solids/gases as well as the total pressure in the bed is determined as a function of bed height using Eqs. (12), (13), (19), (45)–(47)).

An iterative scheme is employed for the above calculations so that we can obtain a self-consistent set of data defining the conditions in the fast and slow beds when steady state prevails in the reactor.

Under steady-state conditions, one can follow the path of oxide and carbon particles through the two legs of the reactor and the extent of reaction of the particles can be calculated. Depending on the residence time distribution for the particles, the extent of reaction will vary and average values can be associated with the prereduced product which is withdrawn continuously at a finite rate.

5. Plant data

Published data on the operation of the CFB for prereduction of iron ores is very limited. Table 1 shows the available prereduction pilot plant data for the ELRED process [6]. The data refer to the fast bed and it is seen that the concentration of solids decreases rapidly in the upper part of the reactor. There is also minimal temperature variation in the reactor. The degree of reduction in the charge is marginally higher at the top (63.7%) than at the bottom of the reactor (60.4%). The reported CO/CO_2 ratio is close to the equilibrium value for the reduction of wüstite by CO, in the whole bed. This indicates that under the reported conditions, the $C-CO_2$ reaction could be rate limiting.

Table 1
Published data on the Elred prereduction Pilot Plant [6]

Parameter	Position in the fast bed		
	Bottom	Middle	Top
Temperature (K)	1243	1263	1253
Solids concentration (kg m^{-3})	600	200	100
Solids composition			
Fe_{total} (wt.%)	57	–	35
Fe_{metal} (wt.%)	25	–	17
C (wt.%)	26	–	55
Gas composition (vol.%)			
CO	33	18	19
CO_2	15	9	10
H_2	6	8	9
CH_4	<1	<1	1

Reactor height: 25 m, gas velocity: 2 m s^{-1}, ore particles: 0.07–0.09 mm, coal particles: 0.2–1 mm, production rate: ~ 450 kg h^{-1}.

Table 2
Parameters used for calculations in the fast bed

Reactor diameter (m)	3.0
Bed height (m)	25.0
Bed temperature (K)	1265
Solids feed	
Recirculation Rate (kg m^{-2} s^{-1})	85
Wt.% C in the feed	25
Total gas pressure at the bottom of the reactor (atm)	5
Fluidizing gas	
Velocity (m s^{-1})	2–3
Composition (vol.%)	
CO	50
CO_2	5
H_2	3.75
H_2O	1.25
N_2	40

Increasing the temperature or the use of a more reactive coal could lower the CO/CO_2 ratios for increasing the driving force for the reduction reaction.

The data reported is by no means complete for carrying out a proper simulation of the process. However, using the published data, two sets of base data are presented in Tables 2 and 3, which have been used in the present calculations.

6. Results and discussion

Fig. 2 shows the variation of selected parameters in the fast bed as a function of gas velocity. Base data used for these calculations are given in Table 2. In the lower regions of the fast bed, bed porosity is affected strongly by changes in gas velocity whereas in the upper regions, porosity approaches unity for the gas velocities considered in the calculations (Fig. 2a). The velocity of solids are shown to approach the gas velocity in the upper regions of the fast bed (Fig. 2b). It is interesting to note that calculated particle velocity in Fig. 2b exceeds the inlet gas velocity in the upper region. This behaviour may be attributed to the estimation of the elutriation flux using the present correlations.

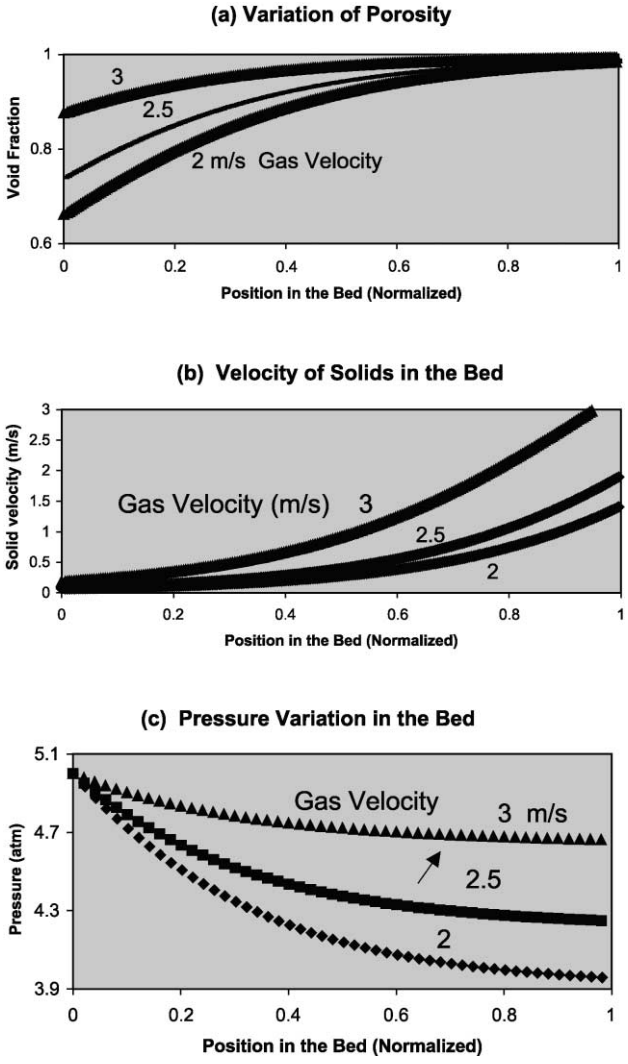

Fig. 2. Variation of selected parameters in the fast bed.

Table 3
Parameters used for calculations in the slow bed

Reactor diameter (m)	3.0
Bed	
Weight (1000 kg)	160
Height (m)	4.5
Porosity (–)	0.47
Temperature at the top (K)	1265
Solids feed	
Recirculation rate (kg m^{-2} s^{-1})	85
Wt.% C in the feed	25
Average particle size (mm)	
Iron oxide	0.08
Coal	0.50
Total gas pressure at the bottom of the reactor (atm)	5
Inlet gas	
Composition (vol.%)	
CO	50
CO_2	5
H_2	3.75
H_2O	1.25
N_2	40
Flow Rate (mol m^{-2} s^{-1})	0.10
Velocity (m s^{-1})	0.02

We have the local solids velocity $= E_h/[\rho_s(1-\varepsilon_h)]$.

Rhodes and Geldart [27] have pointed out that the solids fraction in the dilute phase tends to be underestimated and correlations better suited to the high gas velocities are needed to get over the problem.

In Fig. 2c, as expected, the pressure drop in the bed is larger at relatively lower gas velocities.

Fig. 3 shows the variation of fraction oxygen in the fast bed and CO_2/CO ratio in the gas phase. At higher gas velocities, the CO_2/CO ratio is lower and the gas is more reducing (Fig. 3a). But, the velocity of solids is higher and consequently the residence time for the particles in the fast

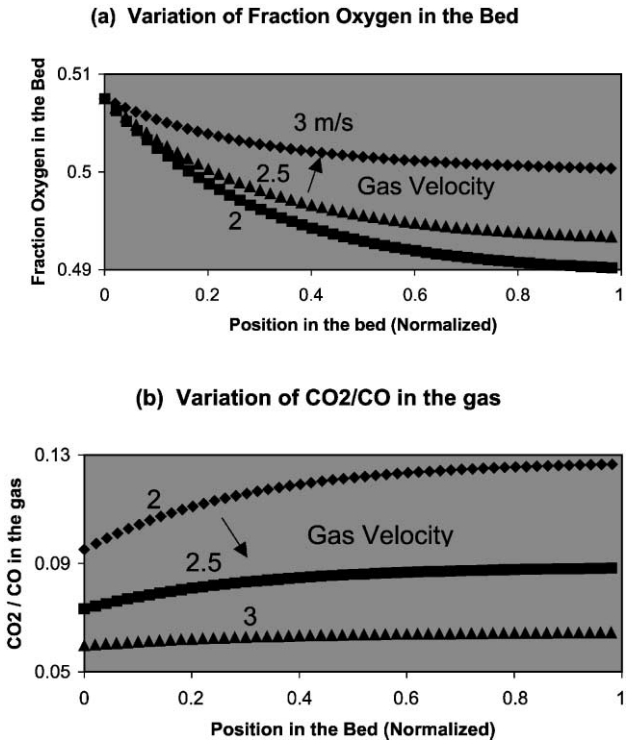

Fig. 3. Variation of fraction oxygen in the fast bed and CO_2/CO in the gas phase.

bed is lower, which leads to lower reduction levels (Fig. 3a). Equilibrium [35,36,42,43] and kinetic data [35,44,45] used for these calculations are given in Tables 4 and 5.

Table 5
Kinetic parameters[a] used in the calculations

Gasification of carbon	
Rate constants	
k_{ct} (kmol kg^{-1} s^{-1})	$2.0\cdot10^4 \exp(-29{,}700/T)$
k'_{ct} (kmol kg^{-1} s^{-1})	$3.2\cdot10^4 \exp(-29{,}700/T)$
Reduction of iron oxide	
Rate constants	
$k_r^{(CO)}$ (m s^{-1}) $Fe_xO \rightarrow Fe$	$4.0 \exp(-10{,}065/T)$
$k_r^{(H2)}$ (m s^{-1}) $Fe_xO \rightarrow Fe$	$11.38 \exp(-10{,}065/T)$
Product layer porosities[b]	
$\varepsilon_m = 0.008 + 0.992\varepsilon_h$	
$\varepsilon_w = 0.122 + 0.878\varepsilon_h$	
$\varepsilon_{Fe} = 0.435 + 0.565\varepsilon_h$	

[a] Refs. [35,44,45].

[b] ε_h is the initial porosity in the hematite particle. ε_m, ε_w and ε_{Fe} correspond to the porosities in magnetite, wüstite and the iron layers. The tortuosity factors in the product layers have been taken to be equal to 2.

In Figs. 2 and 3, the feed and discharge rates have been held constant so that the variation of several parameters, including the degree of reduction could be studied as a function of gas velocity. However, in a process simulation, it is important to think about adjustments in feed and discharge rates in order to achieve the same degree of reduction in the product.

The variation of selected parameters in the slow bed is shown in Fig. 4. Base data used for these calculations are given in Table 3. Equilibrium and kinetic data used are presented in Tables 4 and 5. Assuming no heat losses, a temperature gradient of about 25 K exists between the top

Table 4
Equilibrium data[a] used in the calculations

Gasification of carbon	
$\log_{10}(I_2, \text{atm}^{-1})$	$-8.5306 + 13280/T$
I'_2 (atm^{-1})	35
$\log_{10}(I_3, \text{atm}^{-1})$	$-4.8697 + 8272/T$
$\log_{10}(I'_3, \text{atm}^{-1})$	$3.8530 - 5200/T$

Water gas shift reaction

$CO(g) + H_2O(g) = CO_2(g) + H_2(g)$

The equilibrium constant is given by:

$\log_{10}(K) = -1.5234 + 2.7226 \cdot 10^{-4}T - 0.0854\ln(T) + 1999.4/T$

Reduction of Iron oxide by carbon monoxide or hydrogen

$3Fe_2O_3 + CO(\text{or } H_2) = 2Fe_3O_4 + CO_2(\text{or } H_2O)$ [1]

$x/(4x-3)Fe_3O_4 + CO(\text{or } H_2) = 3/(4x-3)Fe_xO + CO_2(\text{or } H_2O)$ [2]

$Fe_xO + CO(\text{or } H_2) = xFe + CO_2(\text{or } H_2O)$ [3]

$\Delta G^0 = A + BT + CT\ln T + DT^2 \quad (J\ mol^{-1})$

Reaction		A	B	C	D·1000
[1]	CO	12,449.9	−540.87	68.96	−37.55
	H_2	58,655.5	−671.53	81.83	−38.96
[2]	CO	90,039.7	−793.75	106.77	−40.52
	H_2	135,080.0	−909.02	117.43	−40.90
[3]	CO	−41,936.0	230.62	−28.07	8.41
	H_2	3351.8	112.06	−16.94	7.81

[a] Refs. [35,36,42,43].

and bottom of the slow bed (Fig. 4a). The variation of CO_2/CO in the bed is shown as a function of bed height in Fig. 4b. Purely reducing gas entering at the bottom of the bed has a low CO_2/CO ratio. As the gas ascends, the reduction and gasification reactions, the ratio increases and attains a steady value very quickly, at 10% of the total bed height.

The decrease in fractional oxygen in the bed and in an isolated wüstite particle during its first passage through the slow bed is shown in Fig. 4c. The change in fraction oxygen is numerically small, but significant. Fig. 4d shows the variation of gas flow in the bed. The gas flow increases from the finite assumed value of $0.1 \cdot 10^{-4}$ to about $0.13 \cdot 10^{-2}$ mol m^{-2} s^{-1} at the top of the bed.

As mentioned earlier, it has been assumed in this work that the iron ore particles, fed into the CFB reactor through the cyclone, correspond to wüstite. Fig. 5 shows the passage of such a wüstite particle through the slow and fast beds of the circulating fluidized bed reactor and how its oxygen content decreases during its transit. From the figure, it is seen that the oxide particle has to pass through the slow and fast beds about six times before the oxygen content is reduced by 40%. When the CFB reactor is used for the prereduction of iron ores, a reduction level of about 50% to 60% (from hematite) is desired. This would correspond to fraction oxygen in the wüstite in the range 0.75 to 0.6. Thus, under the reactor conditions considered, a freshly introduced iron oxide particle has to circulate in the reactor five to six times for the reduction level to approach 60%.

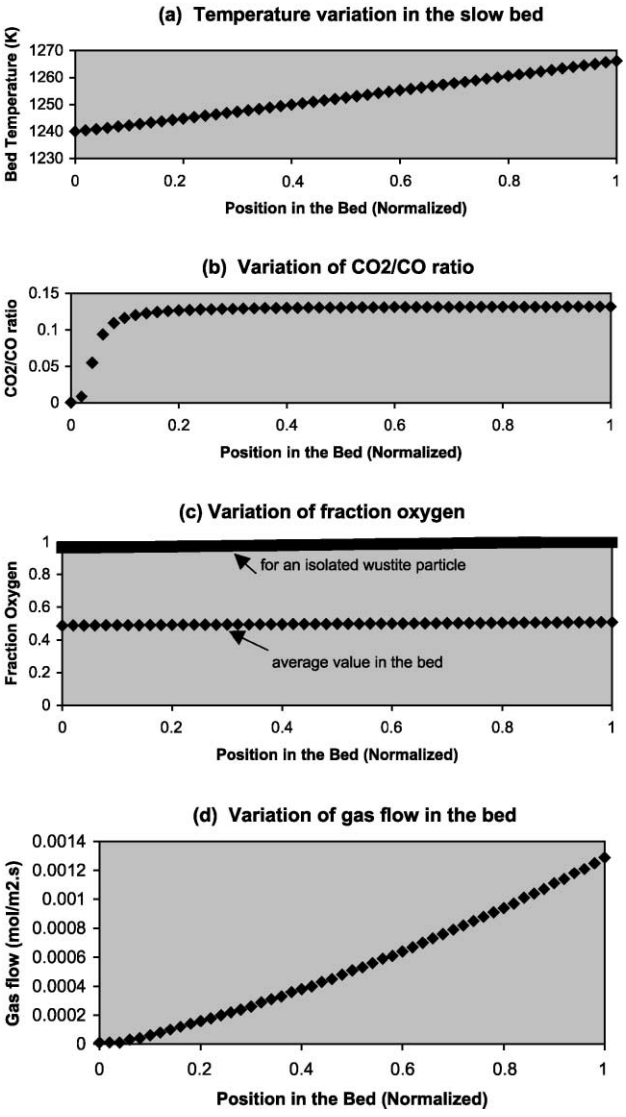

Fig. 4. Variation of selected parameters in the slow bed.

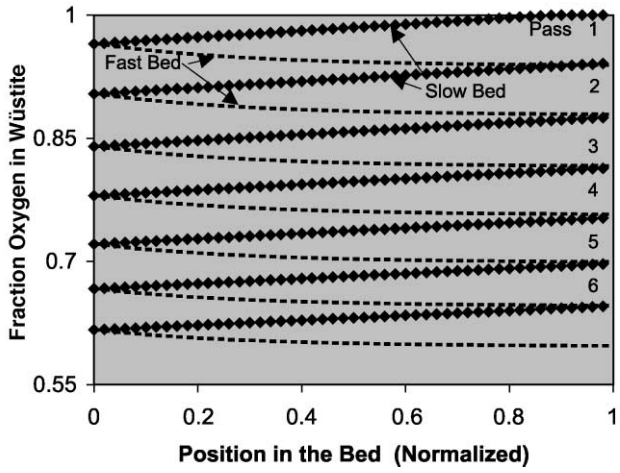

Fig. 5. Reduction of a wüstite particle during its passage through the slow and fast beds of the circulating fluidized bed reactor.

7. Summary

The reduction of iron oxides by carbon in a circulating fluidized bed reactor has been studied. A theoretical analysis has been made which takes into account the fast fluidization of iron oxide and coal particles in the main column by a hot stream of reducing gases. Kinetic and hydrodynamic factors in the reactor are considered and the rate of iron oxide reduction as well as gasification rates for carbon have been calculated.

Using reported base data, the temperature and composition profiles in the charge as well as the gas phase have been calculated using the model, both in the main as well as return columns. Under these conditions, the passage of a freshly introduced iron oxide particle through the CFB reactor has been simulated. Calculations have shown that the oxide particle needs to pass through the fast and slow beds five to six times before a reduction level of about 60% can be achieved.

Notation

a	exponent in Eq. (22)
A_0	area of the distributor plate per orifice, m^2
A_{fb}	cross-sectional area of the fast bed, m^2
A_{sb}	cross-sectional area of the slow bed, m^2

C_0 density of oxygen in the unreduced oxide particle, kg-mol m^{-3}
C_f free site on the carbon surface
C(O) occupied site on the carbon surface
$d_{b,h}$ average bubble diameter in the bed, at a height 'h' above the distributor plate, m
d_p average particle diameter, m
D_{fb} diameter of the fast bed, m
D_{sb} diameter of the slow bed, m
$D_{i,m}$ diffusivity of ith gaseous species in the multicomponent system, $m^2\ s^{-1}$
$D^{eff}_{i,m}$ effective diffusivity of ith gaseous species in the multicomponent system, $m^2\ s^{-1}$
E entrainment flux at the fast bed outlet, kg $m^{-2}\ s^{-1}$
E_0 entrainment flux at the dense phase/dilute phase interface, kg $m^{-2}\ s^{-1}$
E_∞ entrainment flux at TDH, kg $m^{-2}\ s^{-1}$
f_0 fraction of the removable oxygen remaining in the oxide
g acceleration due to gravity, m s^{-2}
G circulation flux of solids, kg $m^{-2}\ s^{-1}$
h height above the dense phase, m
h^* distance between the fast bed outlet and the dense phase/dilute phase interface, m
h_{fb} height of the fast bed, m
h_{sb} height of the slow bed, m
I_2, I_3 rate constants associated with the $C-CO_2$ reaction, atm^{-1}
I'_2, I'_3 rate constants associated with the $C-H_2O$ reaction, atm^{-1}
k_{ct}, k'_{ct} characteristic rate constants for $C-CO_2$ and $C-H_2O$ reactions, $kg^{-1}\ s^{-1}$
$k^{(i)}_{OV}$ overall reaction rate constant for the reducing gas species i, as defined in Eq. (11), m s^{-1}
$k^{(i)}_r$ first-order specific reaction rate constant for the reduction of iron oxide to the next lower oxide or iron by the reducing species i, m s^{-1}
$K^{(i)}_{eq}$ equilibrium constant for the first-order reduction reaction of iron oxide with reducing gas i
M_{den} mass of solids in the dense phase (fast bed), kg
M_{dil} mass of solids in the dilute phase (fast bed), kg
M_{fb} mass of solids in the fast bed, kg
M_{sb} mass of solids in the slow bed, kg
$\dot{n}_O$ rate of oxygen removal in the gaseous reduction of iron oxide particles, kg-at s^{-1}
p^b_i partial pressure of ith gaseous species in the bulk, atm (1 atm = 101,325 Pa)
P_T total pressure, atm
r_0 particle radius, m
r_i instantaneous radial position of the reaction front, m
R gas constant, m^3 atm kg-$mol^{-1}\ K^{-1}$
Re_p particle Reynolds number
$Re_{p,c}$ critical particle Reynolds number
T Temperature, K
U_0 fluidizing gas velocity, m s^{-1}
U_{high} minimum fluidization velocity for one of the solid components in the bed (higher value), m s^{-1}
U_{low} minimum fluidization velocity for one of the solid components in the bed (lower value), m s^{-1}
U_{mf} minimum fluidization velocity for the mixture of solids, m s^{-1}
U_t average terminal velocity for the solids, m s^{-1}
x_{high} wt. fraction of the solid component having the higher minimum fluidization velocity, (–)
X_i mole fraction of ith gaseous species

Greek letters

α parameter defined by Eq. (8)
β parameter defined by Eq. (9)
δ bubble fraction in the dense phase region
ε_b voidage in the bubble phase
ε_{den} voidage in the dense phase region
ε_e voidage in the emulsion phase
ε_{mf} voidage in the bed at minimum fluidization
μ_g average viscosity of the gas mixture, N s m^{-2}
ρ_g average density of gas, kg m^{-3}
ρ_s average density of solids, kg m^{-3}

Subscripts

b bubble phase
cyc cyclone
den dense phase
e emulsion phase
fb fast bed
g gas
mf min. fluidization
p particle
pl product layer
s solid
sb slow bed

References

[1] B.C. Cunningham, J.G. Stephenson, in: R.L. Stephenson (Ed.), Direct Reduced Iron, The Iron and Steel Soc. AIME, Warrendale, 1980, pp. 89–95.
[2] P.R. Dawson, G. Wightman, D. Naden, Proc. ARTIS-88 Conf., Jamshedpur, 1988.
[3] S. Santén, H. Herlitz, B. Flink, J. Skogberg, MINTEK '50, Johannesburg, 1984.
[4] Kawasaki Steel Newsletter (5) (1983) 2.
[5] P. Collin, H. Stickler, Iron Steel Int. (1980) 81–86.
[6] E. Bengtsson, B. Widell, I&SM (October 1981) 30–34.
[7] P. Weber, M. Hirsch, W. Bresser, R. Husain, Proc. Ironmaking Conf., 1994, pp. 491–498.
[8] M. Hirsch, R. Husain, P. Weber, H. Eichberger, Internat. Conf. on Prereduced Products and Europe, Milan, September 1996.

[9] R. Husain, Metal Bulletin's 4th Elec. Furnace Raw Materials Seminar, Zurich, April 2000.
[10] K. Knop, Stahl Eisen 120 (11) (2000) 57–66.
[11] L. Reh, Personal communication, July 2001.
[12] N.S. Srinivasan, L.-I. Staffansson, Chem. Eng. Sci. 45 (1990) 1253–1265.
[13] J. Yerushalmi, in: D. Geldart (Ed.), Gas Fluidization Technology, Wiley, New York, 1986, pp. 155–196.
[14] K. Yoshida, K. Mineo, H. Mineo, in: L.K. Doraiswamy, A.S. Majumdar (Eds.), Transport in Fluidized Particle Systems, Elsevier, New York, 1989, pp. 241–285.
[15] L. Reh, in: P. Basu (Ed.), Circulating Fluidized Bed Technology, Pergamon, Canada, 1986, pp. 105–118.
[16] L. Reh, Chem. Eng. Process. 21 (3) (1986) 117–127.
[17] J.R. Grace, C.J. Lim, C.M.H. Brereton, J. Chaouki, in: R.A. Mashelkar, R. Kumar (Eds.), Reactions and Reaction Engineering, Indian Academy of Sciences, Bangalore, 1987, pp. 35–48.
[18] R.J. Dry, I.N. Christensen, C.C. White, Powder Technol. 52 (1987) 243–250.
[19] P. Basu, C. Ritchie, P.K. Halder, in: P. Basu (Ed.), Circulating Fluidized Bed Technology, Pergamon, Canada, 1986, pp. 229–237.
[20] J.R. Grace, in: P. Basu (Ed.), Circulating Fluidized Bed Technology, Pergamon, Canada, 1986, pp. 63–81.
[21] L. Strömberg, Proc. 7th Internat. Fluidized Bed Combustion Conf., vol. 2, 1982, pp. 1152–1163.
[22] D. Subbarao, P. Basu, Int. J. Heat Mass Transfer 29 (1986) 487–489.
[23] H.S. Mickley, D.F. Fairbanks, AIChE J. 1 (1955) 374–384.
[24] D. Subbarao, P. Basu, in: P. Basu (Ed.), Circulating Fluidized Bed Technology, Pergamon, Canada, 1986, pp. 281–286.
[25] P. Basu, P.K. Nag, An investigation into heat transfer in circulating fluidized beds, Report — Centre for Energy Studies, Technical Univ. of Nova Scotia, Canada, 1986.
[26] Y. Li, M. Kwauk, Proc. 3rd Internat. Fluidization Conf., New Hampshire, USA, 1980, pp. 537–544.
[27] M.J. Rhodes, D. Geldart, Powder Technol. 53 (1987) 155–162.
[28] M.J. Rhodes, D. Geldart, Chem. Eng. Res. Des. 67 (1989) 20–29.
[29] V.W. Weiss, F.N. Fett, K. Helmrich, K. Janssen, Chem. Eng. Process. 22 (1987) 79–90.
[30] T.S. Yun, Trans. ASM 54 (1961) 129–142.
[31] H.Y. Sohn, J. Szekely, Chem. Eng. Sci. 27 (1972) 763–778.
[32] M. Ishida, M. Wen, C.Y. Wen, AIChE J. 14 (1968) 311–317.
[33] R.H. Spitzer, F.S. Manning, W.O. Philbrook, Trans. Met. Soc. AIME 236 (1966) 726–742.
[34] P.L. Walker Jr., F. Rusinko Jr., L.G. Austin, Adv. Catal. 11 (1959) 134–221.
[35] S. Ergun, J. Phys. Chem. 60 (1956) 480–485.
[36] M. Mentser, S. Ergun, Carbon 5 (1967) 331.
[37] J.L. Johnson, in: M.A. Elliott (Ed.), Chemistry of Coal Utilisation, Second Suppl. Vol., John Wiley, New York, 1981, pp. 1491–1598.
[38] L.Y.-L. Cheung, A.W. Nienow, P.N. Rowe, Chem. Eng. Sci. 29 (1974) 1301.
[39] A.W. Nienow, T. Chiba, in: J.F. Davidson, R. Clift, D. Harrison (Eds.), Fluidization, 2nd edn., Academic Press, London, 1985, pp. 357–382.
[40] C.Y. Wen, L.H. Chen, AIChE J. 28 (1982) 117–128.
[41] R.C. Darton, R.D. La Nauze, J.F. Davidson, D. Harrison, Trans. Inst. Chem. Eng. 55 (1977) 274–280.
[42] Y.K. Rao, B.P. Jalan, Met. Trans. 3 (1972) 2465–2477.
[43] HSC Chemistry for Windows, version 4.0, Outokumpu OY, Finland, 1999.
[44] Q. Tsay, W.H. Ray, J. Szekely, AIChE J. 22 (1976) 1064–1079.
[45] T. Murayama, Y. Ono, Y. Kawai, Trans. Iron Steel Inst. Jpn. 18 (1978) 780.